



## High-accuracy SNV calling for bacterial isolates using deep learning with AccuSNV

Herui Liao, Arolyn Conwill, Ian Light-Maka, et al.

*Genome Res.* published online July 6, 2026

Access the most recent version at doi:[10.1101/gr.281341.125](https://doi.org/10.1101/gr.281341.125)

---

<b>P&lt;P</b>	Published online July 6, 2026 in advance of the print journal.
<b>Accepted Manuscript</b>	Peer-reviewed and accepted for publication but not copyedited or typeset; accepted manuscript is likely to differ from the final, published version.
<b>Open Access</b>	Freely available online through the <i>Genome Research</i> Open Access option.
<b>Creative Commons License</b>	This manuscript is Open Access. This article, published in <i>Genome Research</i> , is available under a Creative Commons License (Attribution-NonCommercial 4.0 International license), as described at <a href="http://creativecommons.org/licenses/by-nc/4.0/">http://creativecommons.org/licenses/by-nc/4.0/</a> .
<b>Email Alerting Service</b>	Receive free email alerts when new articles cite this article - sign up in the box at the top right corner of the article or <a href="#">click here</a> .

---

**Comprehensive** immune receptor profiling.  
Discover the **DriverMap™ AIR Assay** difference.

LEARN  
MORE



---

To subscribe to *Genome Research* go to:  
<https://genome.cshlp.org/subscriptions>

---

Published by Cold Spring Harbor Laboratory Press

# 1 High-accuracy SNV calling for bacterial isolates using 2 deep learning with AccuSNV

3 Herui Liao<sup>1,2</sup>, Arolyn Conwill<sup>1,2</sup>, Ian Light-Maka<sup>5,6</sup>, Martin Fenk<sup>5,7</sup>, Alyssa H. Mitchell<sup>1,2</sup>,  
4 Evan B. Qu<sup>1,2</sup>, Paul Torrillo<sup>1,2</sup>, Jacob S. Baker<sup>1,2</sup>, Lilly R. Bartsch<sup>5</sup>, Felix M. Key<sup>5</sup>, Tami  
5 D. Lieberman<sup>1,2,3,4,\*</sup>

6 • <sup>1</sup> Institute for Medical Engineering and Sciences, Massachusetts Institute of  
7 Technology; Cambridge, MA 02139, USA

8 • <sup>2</sup> Department of Civil and Environmental Engineering, Massachusetts  
9 Institute of Technology; Cambridge, MA 02139, USA

10 • <sup>3</sup> Broad Institute of MIT and Harvard; Cambridge, MA 02139, USA

11 • <sup>4</sup> Ragon Institute of MGH, MIT, and Harvard; Cambridge, MA 02139, USA

12 • <sup>5</sup> Max Planck Institute for Infection Biology; Berlin 10117, Germany

13 • <sup>6</sup> Charité-Universitätsmedizin Berlin, Berlin 10117, Germany

14 • <sup>7</sup> Humboldt-Universität zu Berlin, Faculty of Life Sciences, Berlin, Germany

15 • \* Corresponding author. Email: [tami@mit.edu](mailto:tami@mit.edu)

## 16 Abstract

17 Accurate detection of mutations within bacterial species is critical for fundamental  
18 studies of microbial evolution, reconstructing transmission events, and identifying  
19 antimicrobial resistance mutations. While many tools have been developed to  
20 identify single nucleotide variants (SNVs) from whole-genome sequencing, they  
21 often suffer from high false positive rates due to the complexity of bacterial  
22 genomes and the need for different filtering cutoffs across sample types and  
23 sequencing depths. As datasets increase in size, the manual filtering required for  
24 high accuracy presents a significant obstacle. Here, we present AccuSNV, a novel  
25 deep learning-based tool for high-precision and automated bacterial SNV calling.  
26 Unlike traditional methods that process one sample at a time, AccuSNV leverages a  
27 convolutional neural network (CNN) that integrates alignment information across  
28 multiple samples, enhancing precision through learned across-sample patterns.  
29 We evaluate AccuSNV against seven popular SNV calling tools using simulated data  
30 from six bacterial species with varied sequencing depths, numbers of isolates,  
31 mutations, and divergence levels. To further validate its real-world utility, we test  
32 AccuSNV on multiple curated bacterial datasets containing reported SNVs. In both  
33 simulated and real-world scenarios, AccuSNV consistently achieves the best  
34 performance. Moreover, AccuSNV provides comprehensive user-friendly  
35 downstream analysis modules and outputs, including mutation annotation  
36 information, phylogenetic inference,  $d_N/d_S$  calculations, and optional manual

37 filtering. Together with the automated deep learning–based calling, these features  
38 make AccuSNV broadly accessible to users with different levels of computational  
39 expertise.

40

---

## 41 Introduction

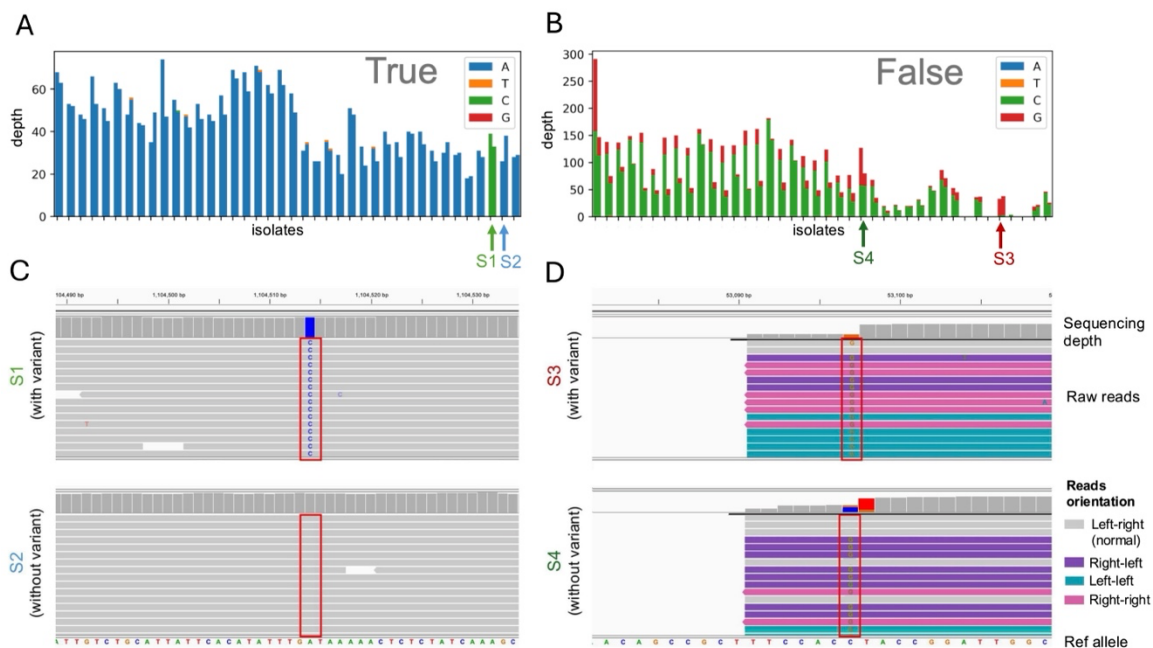
42 Single nucleotide variants (SNVs), single-base substitutions in a genome, represent  
43 the most common form of genetic variation. In bacteria, accurate identification of  
44 SNVs is a critical step in connecting genetic variation to phenotype (Lopatkin et al.  
45 2021; Schrader et al. 2021) and for reconstructing bacterial evolution (Barrick et al.  
46 2009). In particular, SNV mutations form the basis of most phylogenetic inference  
47 approaches, making their accurate detection essential for epidemiology (Halachev  
48 et al. 2014). Even small errors in SNV detection can have outsized effects on  
49 downstream analyses. This is especially true for many bacterial species, which  
50 accumulate SNV mutations at a rate of only 1 - 10 SNVs per genome per year (Key et  
51 al. 2023). This low rate of mutation accumulation makes evolutionary inference  
52 methods sensitive to false positives, thus requiring high-precision SNV calling.

53 SNV calling across bacterial genomes of the same species remains a challenging  
54 task. One major source of SNV calling errors arises from alignment inaccuracies,  
55 which are exacerbated by the high diversity within bacterial species. Unlike the  
56 relatively stable and homogeneous human genome, bacteria within the same  
57 species can vary up to 5% in nucleotide identity and share only 40% of their gene  
58 content. These characteristics increase the possibility of misalignments and false  
59 variant calls (Zojer et al. 2017), particularly in low-coverage datasets or when the  
60 sample strain diverges from the reference genome (Bush et al. 2020). In addition,  
61 cross-contamination during high-throughput sequencing preparation can lead to  
62 false positive and false negative SNV calls, posing challenges for standard  
63 mapping-based SNV filtering methods (Goig et al. 2020). These errors can  
64 significantly reduce the precision of bacterial SNV calling.

65 Several SNV calling tools have been developed and applied to identify SNVs across  
66 bacterial isolates (Li et al. 2009; Koboldt et al. 2009; McKenna et al. 2010; Garrison  
67 and Marth 2012; Barrick et al. 2014; Seemann 2015; Yoshimura et al. 2019). Most of  
68 these tools combine probabilistic models (likelihoods or statistics) for each  
69 genotype in each sample based on alignment metrics such as base quality, read  
70 depth, and strand bias, and then apply filters or thresholds to make allele calls in  
71 per-sample basis. Some of these tools, such as GATK and FreeBayes, were  
72 originally designed for eukaryotic organisms like humans (McKenna et al. 2010) and  
73 are not specifically optimized for bacterial genomes, while others like breseq and  
74 Snippy are tailored for microbial analysis. These methods are widely used due to  
75 their simplicity and informative visualizations that support additional filtering as

76 needed. A second category integrate both mapping and assembly information. For  
 77 example, BactSNP, performs *de novo* assembly of input reads and aligns the  
 78 assembled contigs to the reference genome to identify SNVs. Through this  
 79 approach, BactSNP aims to reduce false positives caused by read misalignment in  
 80 complex genomic regions. However, the accuracy of this approach depends heavily  
 81 on the quality of the assembly and the similarity between sample and reference  
 82 genomes, and it remains computationally intensive for large datasets  
 83 (Supplementary Table S1).

84 Despite their respective strengths, these existing methods share common  
 85 limitations. First, most tools typically call variants by considering each isolate  
 86 individually, which obscures across-sample patterns that can reveal systematic  
 87 alignment errors at specific genomic positions. False SNVs emerging from  
 88 alignment errors exhibit distinct alignment patterns across samples (Fig. 1A-1D),  
 89 and failing to consider these patterns while focusing solely on single-sample  
 90 evidence can lead to false-positive calls. Another common issue is reference bias:  
 91 when all samples share a nucleotide that differs from the reference, methods that  
 92 do not consider raw read data may erroneously call the site as polymorphic (e.g.  
 93 where the reference nucleotide stems from low-coverage assembly errors),  
 94 resulting in false positives. Lastly, these tools rely on manually defined thresholds  
 95 or assumptions that may not generalize well, and often require extensive manual  
 96 filtering to reduce false positives.



97

98 **Figure 1. False SNVs arising from alignment errors are detectable from across-**  
 99 **sample patterns (A-B):** Bar charts show sequencing depth across isolates for an  
 100 example true SNV (A) and a false SNV (B) from real-world clinical data, with each  
 101 pair of bars representing reads aligned to the forward and reverse strands for a

102 *single isolate, colored by nucleotide supported. Arrows indicate two randomly*  
103 *selected isolates (S1, S2 for the true SNV; S3, S4 for the false SNV) that are shown in*  
104 *(C) and (D). (C-D): Integrative Genomics Viewer (IGV) views of the selected*  
105 *representative isolates S1, S2 (C) and S3, S4 (D) carrying either the major or*  
106 *alternative allele for the true and false SNV, respectively. The candidate SNV*  
107 *position is highlighted by red boxes, with the reference allele shown at the very*  
108 *bottom of the figure. In panel D, the false positive arises from systematic mis-*  
109 *mapping of reads to this genomic position in both samples. The presence of a*  
110 *nearby structural variant results in the preferential recruitment of erroneous reads,*  
111 *leading to a variant call in the absence of sufficient reference allele support. Reads*  
112 *are colored by pair orientation. Only left–right orientation (with the upstream read on*  
113 *the forward strand and downstream read on the reverse strand) is considered*  
114 *normal; abnormal orientations often indicate alignment errors or structural variants.*

115

116 These constraints limit precision and scalability, particularly in studies involving  
117 low-depth sequencing, high strain diversity, or large-scale comparative analyses.  
118 Recent advances in deep learning (Min et al. 2016; Hernández Medina et al. 2022;  
119 Liao et al. 2023) have opened new possibilities for addressing these limitations.  
120 Unlike traditional rule-based or statistical approaches, deep learning models can  
121 automatically learn complex patterns from raw input data (Ahmed et al. 2023). In  
122 the context of bacterial SNV calling, this allows models to move beyond fixed  
123 thresholds and handcrafted features, instead identifying informative signals directly  
124 from sequencing alignments. Importantly, deep learning architectures, such as  
125 convolutional neural networks (CNNs), are well-suited to capture both local  
126 alignment features and broader patterns across samples, offering a powerful  
127 framework for distinguishing true variants from false positives in diverse and noisy  
128 datasets.

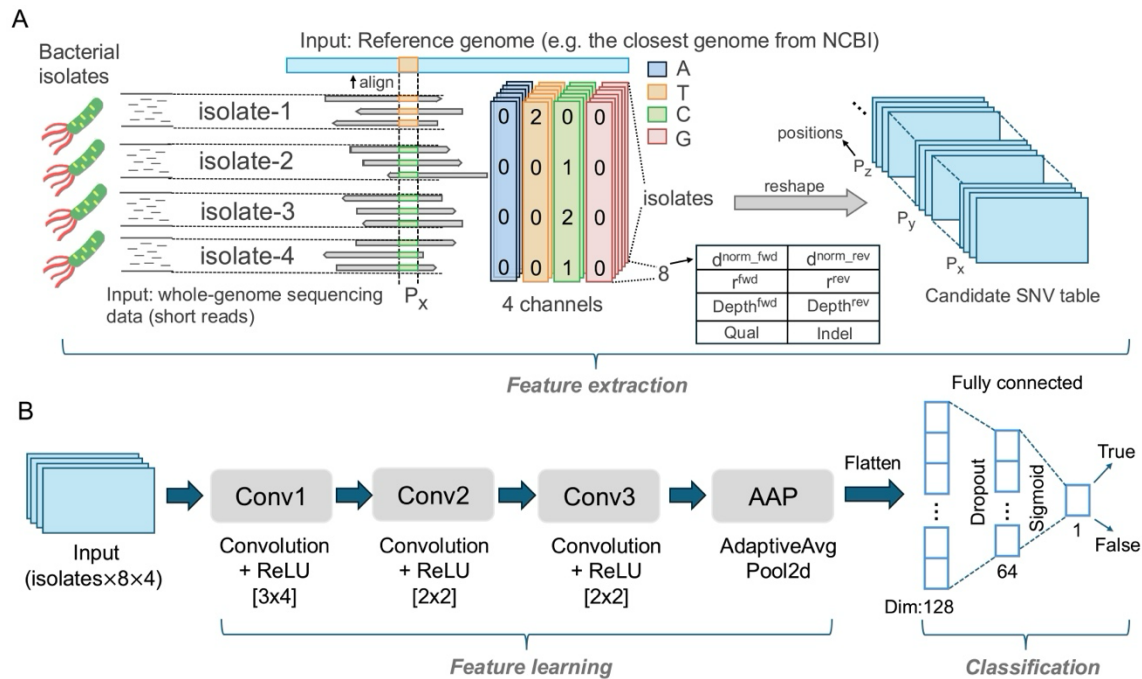
129 In this work, we have developed AccuSNV, a deep learning-based SNV calling tool  
130 optimized for bacterial whole-genome sequencing (WGS) data. AccuSNV leverages  
131 a unique data structure that summarizes across-sample alignment information at  
132 each candidate SNV and a CNN model that derives informative patterns from this  
133 multisample read alignment data. By capturing both within-sample signals and  
134 across-sample patterns, it offers improved robustness to low-depth coverage,  
135 reference and genome divergence, and diverse real-world datasets. AccuSNV takes  
136 a reference genome and raw short-read WGS data from multiple ( $\geq 3$ ) isolates as  
137 input, and outputs high-confidence SNVs alongside predicted probabilities, variant  
138 annotations, per-sample allele calls, and informative visualizations. Through  
139 comprehensive benchmarking across both simulated and real-world datasets, we  
140 show that AccuSNV achieves consistently superior precision and generalization  
141 across a wide range of bacterial species and sequencing conditions.

## 142 Results

### 143 AccuSNV employs a CNN model trained on real-world bacterial 144 isolate data

145 In this study, we curated real-world bacterial isolate WGS data (short reads) with  
146 manually labeled SNVs from prior studies conducted by our lab (Zhao et al. 2019;  
147 Conwill et al. 2022; Baker et al. 2025) to serve as training and validation datasets of  
148 AccuSNV. These datasets span 3 different species, with significantly different  
149 genome sizes and GC contents (Supplementary Table S2). We chose this data  
150 because: (1). real-world data contains authentic sequencing noise, technical  
151 artifacts, and biological complexity that are difficult to simulate, providing a more  
152 robust foundation for model training compared to simulated data; (2). validated  
153 SNV datasets are rare, and most publicly available ones report only true positives  
154 without false SNVs, making it impossible for models to learn the features of false  
155 calls. Our lab's datasets overcome this limitation through manual labeling of both  
156 true and false SNVs, with standardized formats and stringent filtering  
157 (Supplementary Table S3); (3). for these datasets, pre-extracted alignment-derived  
158 features were already available, which greatly reduced the time and computational  
159 cost of model training since raw sequencing data did not need to be reprocessed. In  
160 addition, these curated features supported the quick generation of bar charts (Fig.  
161 1) that visually distinguish high-quality from low-quality SNVs, providing an  
162 additional manual validation beyond automated filters (see Methods) and thereby  
163 enhancing label reliability; (4). the diversity of bacterial species and experimental  
164 contexts provides a foundation for generalization. Given these datasets, each  
165 candidate SNV site was encoded as a feature vector summarizing read-level signals  
166 and cross-sample alignment patterns (Fig. 2A), and a CNN was trained to classify  
167 them as true or false variants (Fig. 2B).

168 Critically, alignment error patterns, such as depth imbalances and mixed allelic  
169 signals in false positives, remain consistent across the three species used for  
170 training because false-positives are primarily driven by common failure modes of  
171 short-read sequencing and alignment algorithms (Supplementary Fig. S2). This  
172 observation led us to hypothesize that a model could be built which effectively  
173 generalizes by learning these shared patterns.



174

175 *Figure 2. A deep learning framework that leverages across-sample comparisons for*  
 176 *bacterial SNV calling. (A). Feature extraction pipeline: short reads from bacterial*  
 177 *isolates are aligned to a reference genome, features at candidate SNV positions are*  
 178 *extracted across four channels (A, T, C, G). For each channel, there are 8 features*  
 179 *(see Supplementary Fig. S1 for full details):  $Depth^{fwd}$ ,  $Depth^{rev}$ : raw forward- and*  
 180 *reverse-strand depths;  $d^{norm\_fwd}$ ,  $d^{norm\_rev}$ : forward- and reverse-strand*  
 181 *normalized depths at each locus and each channel;  $r^{fwd}$ ,  $r^{rev}$ : forward- and*  
 182 *reverse-strand relative depths showing the fraction of total coverage contributed by*  
 183 *each isolate at each position and each channel;  $Qual$ : Consensus quality (FQ)*  
 184 *scores produced by SAMtools;  $Indel$ : the number of reads supporting insertions and*  
 185 *deletions at each position in that channel. These features are reshaped into a 4D*  
 186 *(positions  $\times$  isolates  $\times$  features  $\times$  channels) tensor and stored in a candidate SNV*  
 187 *table for neural network input. (B). Model architecture: the input tensor is processed*  
 188 *through three convolutional layers with ReLU activation and varying kernel sizes*  
 189 *(shown in brackets), followed by adaptive average pooling. The output is then*  
 190 *flattened and passed through fully connected layers with dropout for binary*  
 191 *classification. The model finally outputs prediction probabilities, with SNVs*  
 192 *classified as True if probabilities  $> 0.5$ , otherwise False.*

## 193 The CNN model outperforms classical machine learning methods

194 To build AccuSNV, we first explored several classical machine learning models  
 195 using the labeled SNV dataset derived from read alignments of real bacterial  
 196 sequencing data from the Lieberman Lab. Input features (Supplementary Fig. S1)  
 197 were constructed from read alignment patterns at candidate sites along with  
 198 across-sample alignment statistics, and these were used to train XGBoost, random

199 forest, support vector machines (SVM), and logistic regression models. We  
200 compared their performance against the CNN model with two and three  
201 convolutional layers to determine the optimal model complexity for capturing local  
202 sequence context and across-sample alignment patterns. To minimize bias, we  
203 randomly split the dataset into training and validation sets five times, retrained all  
204 models on each split, and reported average performance metrics on the validation  
205 data (Supplementary Fig. S3).

206 The CNN model consistently achieved the highest scores across all evaluation  
207 metrics on the validation dataset (Supplementary Fig. S3), outperforming all  
208 classical models ( $p < 0.05$ , Wilcoxon signed-rank test). Notably, the three-layer CNN  
209 also outperformed a shallower two-layer CNN architecture, demonstrating the  
210 importance of sufficient model depth for learning complex alignment patterns.

211 To understand which features contribute most to the CNN's performance, we  
212 conducted an ablation study by systematically removing different feature groups,  
213 retraining the model, and evaluating performance on the validation set  
214 (Supplementary Fig. S4). Consensus quality scores (Qual), derived from SAMtools  
215 FQ score, showed the largest impact when removed (0.66% F1 drop), consistent  
216 with their established importance in variant calling. However, removing any other  
217 single feature group resulted in modest performance decreases ( $< 0.4\%$  F1 drop),  
218 indicating that the CNN's robustness stems from integrating multiple  
219 complementary features rather than relying on any single dominant signal.

220 The superior performance of CNN likely stems from fundamental architectural  
221 differences between CNN and classical machine learning approaches in handling  
222 genomic alignment data. Specifically, CNN preserves the relationship between  
223 alleles and their features across samples, while classical models require flattening  
224 to 2D vectors that lose crucial across-sample patterns. Additionally, CNNs can  
225 automatically learn complex patterns from the multidimensional alignment data  
226 and detect recurring motifs (e.g. the same minor allele across many samples, Fig.  
227 1B) regardless of their position in the tensor, whereas classical models rely on  
228 hand-crafted features and cannot capture these spatial relationships. These results  
229 motivated our choice of CNN with 3 convolutional layers as the core of the  
230 AccuSNV framework.

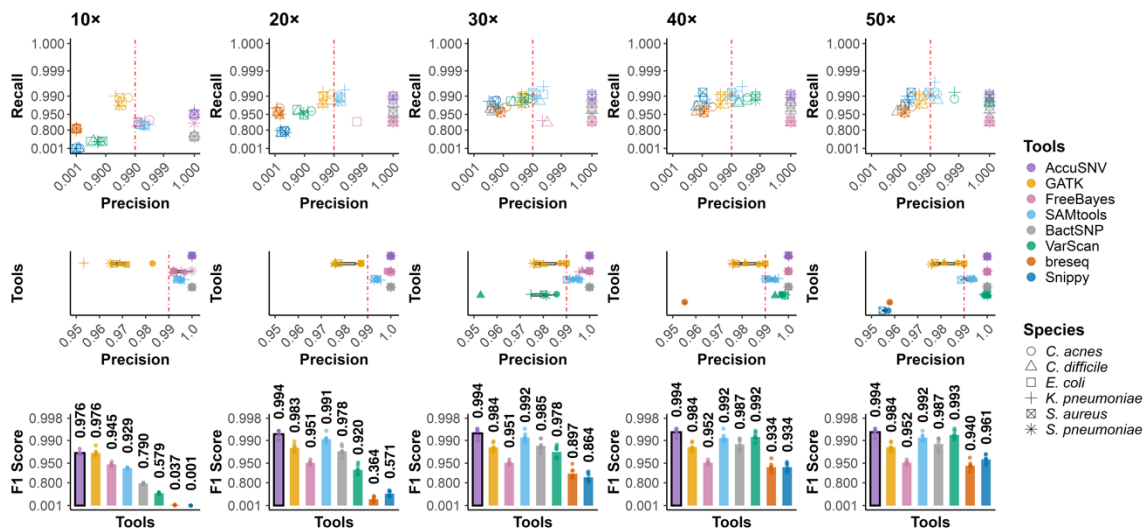
## 231 Overview of benchmark experiments

232 To evaluate the performance of AccuSNV, we benchmarked it against seven widely  
233 used SNV calling tools (GATK v.4.5.0.0, FreeBayes v.1.3.6, SAMtools v.1.20,  
234 BactSNP v.1.1.0, VarScan v.2.4.6, breseq v.0.39.0, and Snippy v.4.6.0) using both  
235 simulated and real-world datasets. The simulated data consisted of Illumina-like  
236 reads generated from six representative bacterial species across a range of  
237 sequencing depths (10× to 50×), divergence levels, and contamination scenarios,  
238 totaling thousands of samples. All tools were run using default or recommended

239 parameters (see Supplementary Section 1). Across these diverse conditions,  
 240 AccuSNV achieved consistently high accuracy, demonstrating robustness to  
 241 challenges including low coverage, reference and genome divergence, and complex  
 242 sequencing and alignment artifacts.

## 243 AccuSNV achieves high precision across sequencing depths

244 Sequencing depth serves as a critical factor influencing the accuracy of SNV calling,  
 245 where low coverage can lead to false positives or missed true SNVs (Fuchs et al.  
 246 2024). In this experiment, we simulated datasets of 10 isolates with sequencing  
 247 depths of 10×, 20×, 30×, 40×, and 50× to compare the performance of different  
 248 tools across varying sequencing depths. First, we selected six representative  
 249 bacterial species (*C. acnes*, *C. difficile*, *E. coli*, *K. pneumoniae*, *S. aureus*, *S.*  
 250 *pneumoniae*) and retrieved representative reference genomes (see Methods) from  
 251 NCBI (Sayers et al. 2024). To mimic real-world scenarios, we simulated datasets of  
 252 closely related organisms and a more distant reference genome. As illustrated in  
 253 Supplementary Fig. S5A, we introduced 1% SNVs and 500 indels into each  
 254 reference genome with SimuG (Yue and Liti 2019) to create a root genome, which  
 255 serves as the common ancestral sequence from which all simulated isolates will  
 256 subsequently diverge. From this, we generated 10 mutant genomes (with about 70  
 257 mutant positions introduced per genome on average) per species with a  
 258 phylogenetic structure intended to mimic realistic evolutionary relationships and  
 259 simulated Illumina reads at 10× to 50× coverage using ART (Huang et al. 2011),  
 260 resulting in 300 samples (10 isolates × 6 species × 5 depths). All reads were aligned  
 261 back to the corresponding reference genome, SNV calling was performed using  
 262 each tool, and precision, recall, and average F1 scores of each tool were calculated  
 263 (Fig. 3).



264

265 **Figure 3. AccuSNV achieves high precision across simulated datasets with**  
 266 **different sequencing depths. Precision, recall, and average F1 scores of AccuSNV**

267 *and seven other variant-calling tools were evaluated across simulated bacterial*  
268 *datasets at five sequencing depths (10×, 20×, 30×, 40×, and 50×). Axes use a*  
269 *transformed scale ( $-\log_{10}(1.0001 - x)$ ) to enhance visualization in the higher range*  
270 *(0.9-1). Shapes represent species and colors represent tools. The vertical line at*  
271 *0.99 precision highlights how more tools achieve high performance at greater*  
272 *sequencing depths. Top panels show precision–recall scatter plots for all tools and*  
273 *species at each depth. Middle panels provide a zoomed-in view of precision*  
274 *distributions across tools and species. Bottom panels summarize the average F1*  
275 *score for each tool. The bar corresponding to AccuSNV is highlighted by a black*  
276 *outline.*

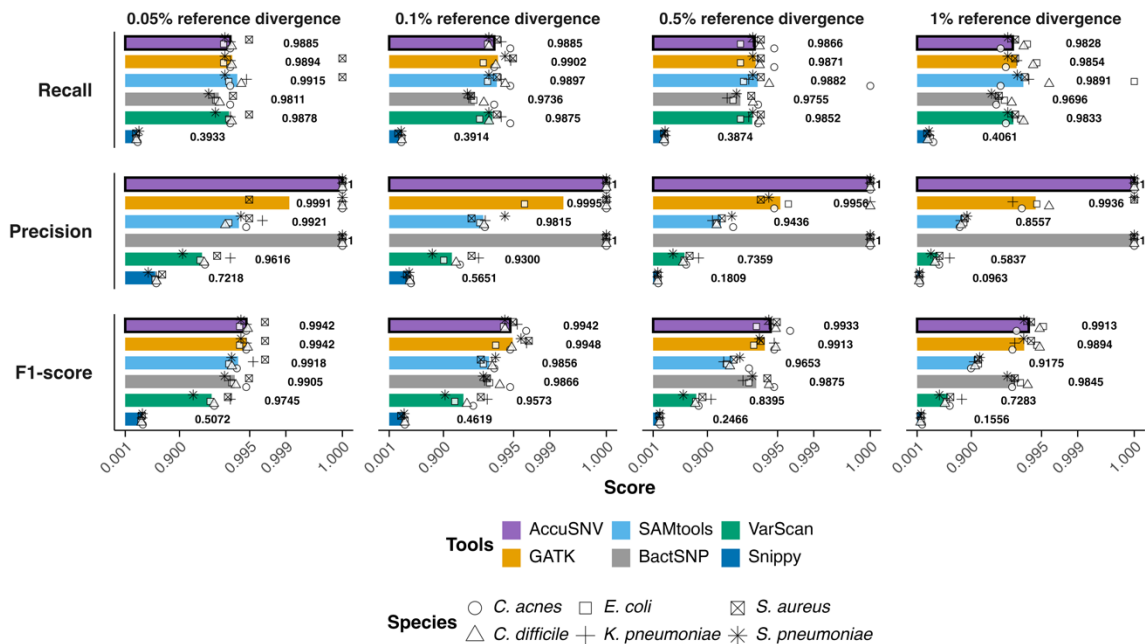
277 The performance of all tools improves with increasing sequencing depth,  
278 highlighting the importance of high-depth sequencing data for existing tools to  
279 accurately identify bacterial SNVs. In addition, AccuSNV achieves the highest  
280 average F1 score across all tested datasets (Fig. 3). In particular, AccuSNV achieves  
281 F1 scores of 97.6% and 99.4% at coverages as low as 10× and 20×, respectively,  
282 while maintaining 100% precision across all experiments. Among other tools,  
283 BactSNP also achieves perfect precision but with lower recall compared to  
284 AccuSNV. At a sequencing depth of 10×, GATK has higher recall than AccuSNV, but  
285 its average precision is 96.8%, compared to 100% for AccuSNV. SAMtools and  
286 VarScan perform competitively at higher depths but underperform at 10×, with F1  
287 scores dropping to 92.9% and 57.9%, respectively. The remaining three tools,  
288 FreeBayes, breseq, and Snippy show poorer performance compared to other tested  
289 tools across all datasets. The performance of both breseq and Snippy drop  
290 markedly at 10× depth, because the conservative filters, such as minimum depth,  
291 allele-fraction and strand-balance requirements, and evidence-count thresholds,  
292 discard many true variants and true reference calls once the effective coverage falls  
293 below these cutoffs.

## 294 **AccuSNV maintains high accuracy on large and noisy simulated** 295 **datasets**

296 In real-world scenarios, sequencing samples from different isolates often have  
297 varying depths and complex phylogenetic relationships. Moreover, previous studies  
298 have shown that the divergence between the target genome and the reference  
299 genome significantly impacts bacterial SNV calling performance (Bush et al. 2020).  
300 Lastly, many real-world datasets contain large isolate collections, introducing  
301 additional complexity to SNV detection. To better reflect these real-world  
302 challenges, we generated an additional large-scale, noisy simulated dataset for  
303 evaluation. Notably, FreeBayes and breseq were excluded from this experiment and  
304 subsequent real-world data evaluations due to their lower accuracy in earlier  
305 evaluations and substantially longer runtimes (Supplementary Table S1).

306 To investigate the influence of the reference genome, we first generated four root  
307 genomes per species of varying reference divergence from the reference genome.

308 From each root genome, we simulated a phylogenetic tree with 100 strains using  
 309 Msprime (Baumdicker et al. 2021), which provided the number of mutations along  
 310 each branch for the given mutation rate (used  $5 \times 10^{-10}$  here). We then assigned  
 311 80% of the mutations as SNVs and 20% as indels, and used SimuG to generate the  
 312 corresponding mutated genomes. We focused solely on SNVs and indels without  
 313 larger recombination or rearrangement events, as this analysis targets very closely  
 314 related isolates where such structural variations are rare. Paired-end reads were  
 315 simulated at random depths between 15 $\times$  and 70 $\times$ . In total, this yielded 2,400  
 316 samples (100 isolates  $\times$  6 species  $\times$  4 reference divergence levels) for evaluating  
 317 SNV calling tools (Supplementary Fig. S5B).



318

319 **Figure 4. AccuSNV maintains high accuracy on large and noisy simulated**  
 320 **datasets.** Performance comparison of six SNV calling tools across four reference  
 321 divergence levels. Axes use a transformed scale ( $-\log_{10}(1.0001 - x)$ ) to enhance  
 322 visualization in the higher range (0.9-1). Shapes represent species and colors  
 323 represent tools. Panels show average recall (top), precision (middle), and F1 score  
 324 (bottom) across all species. AccuSNV bars are highlighted with a black outline.

325 AccuSNV exhibits the most competitive performance among all tested tools, with  
 326 average F1 scores exceeding 99% across all datasets (Fig. 4). It maintains perfect  
 327 precision across all reference divergence levels and achieves an F1 score above  
 328 99.1% even at the highest reference divergence (1%). In contrast, other tools show  
 329 greater variability: VarScan, SAMtools, and Snippy all experience significant drops in  
 330 precision or recall at higher reference divergence levels. Although GATK performs  
 331 comparably to, or slightly better than, AccuSNV at the 0.05% and 0.1% reference  
 332 divergence levels in terms of F1 score, this is driven by increased recall at the cost  
 333 of reduced precision, which is suboptimal when comparing closely-related

334 genomes where precision is critical (Bush 2021). BactSNP also maintains perfect  
335 precision across all datasets but with consistently lower recall, leading to reduced  
336 F1 scores, especially under higher reference divergence.

337 Overall, all tools exhibit decreased performance as the divergence between the root  
338 genome and the reference genome increases, highlighting the growing difficulty of  
339 variant calling when read-reference mismatches become more prevalent. Despite  
340 this, AccuSNV shows minimal performance fluctuation across reference  
341 divergence levels. In addition, tools such as SAMtools and VarScan, which  
342 performed well in the previous experiments with only 10 strains at 50×, uniform  
343 sequencing depth, and simplified phylogenetic structure, showed markedly  
344 reduced performance on this more realistic and noisy dataset. The performance  
345 degradation is particularly pronounced for Snippy, which is sensitive to false-  
346 positive calls under increased reference divergence and noise due to  
347 misalignments near indels and other structural differences (Supplementary Fig. S6)  
348 (Yoshimura et al. 2019). These results indicate that the robustness of existing tools  
349 may decline under more complex and realistic sequencing conditions. In contrast,  
350 AccuSNV maintains both high accuracy and consistency, supporting its use in  
351 large-scale bacterial variant detection across diverse and complex conditions.

352 While the experiment with varying sequencing depths reflects the realistic  
353 heterogeneity commonly observed in bacterial genomics studies, using a uniform  
354 sequencing depth allows us to examine the effect of reference divergence without  
355 the confounding effect of sequencing depth. We therefore conducted an additional  
356 controlled experiment with a uniform sequencing depth of 50× across all isolates to  
357 disentangle the impact of reference divergence from depth variation  
358 (Supplementary Fig. S7). Under this controlled setting, AccuSNV maintains top-tier  
359 performance across all reference divergence levels (0.05%–1%), still achieving F1  
360 scores above 99.1% with perfect precision even at 1% divergence.

### 361 *Experiments on highly variable isolates*

362 Some real-world bacterial populations, such as those from environmental samples,  
363 can exhibit substantial genetic variability between isolates. To evaluate how well  
364 different tools perform under such conditions, we varied the mutation rate in 100 *E.*  
365 *coli* genomes using Mspime (see Supplementary Fig. S5B), based on a root genome  
366 containing 1% sequence variation. Specifically, we tested mutation rates of  
367  $5 \times 10^{-9}$ ,  $5 \times 10^{-8}$ , and  $1 \times 10^{-7}$ , along with the original rate of  $5 \times 10^{-10}$  per site  
368 per generation. We reran all tools on these datasets and recorded the results  
369 (Supplementary Fig. S8).

370 As mutation rates increased, all tools exhibited more false positives and false  
371 negatives. Nevertheless, AccuSNV achieved a high average F1 score (98.85%) by  
372 balancing recall and precision. GATK (with 98.81% average F1 score) showed the  
373 most competitive F1 score at higher mutation rates but had lower precision than  
374 AccuSNV. In contrast, BactSNP (with 98.11% average F1 score) maintained higher

375 precision across all datasets, but its recall was substantially lower. SAMtools (with  
376 98.33% average F1 score) achieved the best recall across all datasets, yet it  
377 produced more false positives at higher mutation rates. Overall, AccuSNV  
378 demonstrated the highly robust and reliable performance across mutation rates,  
379 underscoring its effectiveness for analyzing highly variable bacterial isolates.

## 380 Computational efficiency comparison

381 To compare the running time and memory usage of different tools, we applied all  
382 tools to 10-strain and 100-strain *E. coli* simulated datasets and recorded the  
383 computational performance metrics (Supplementary Table S1). AccuSNV  
384 demonstrated competitive efficiency, completing analysis in 30.3 minutes for 10  
385 isolates (50×) and 64.5 minutes for 100 isolates (15×-70×), with memory usage of  
386 1,140 MB and 1,340 MB respectively. While some tools like Snippy showed faster  
387 execution times (5 minutes on a 10-strain dataset and 50 minutes on a 100-strain  
388 dataset), AccuSNV maintained better performance without the extreme  
389 computational demands observed in tools like FreeBayes and breseq, which failed  
390 to complete within reasonable time limits on the larger dataset (running more than  
391 2 days on the 100-strain dataset). The results demonstrate that AccuSNV provides a  
392 balance between accuracy and computational efficiency for bacterial SNV calling  
393 applications.

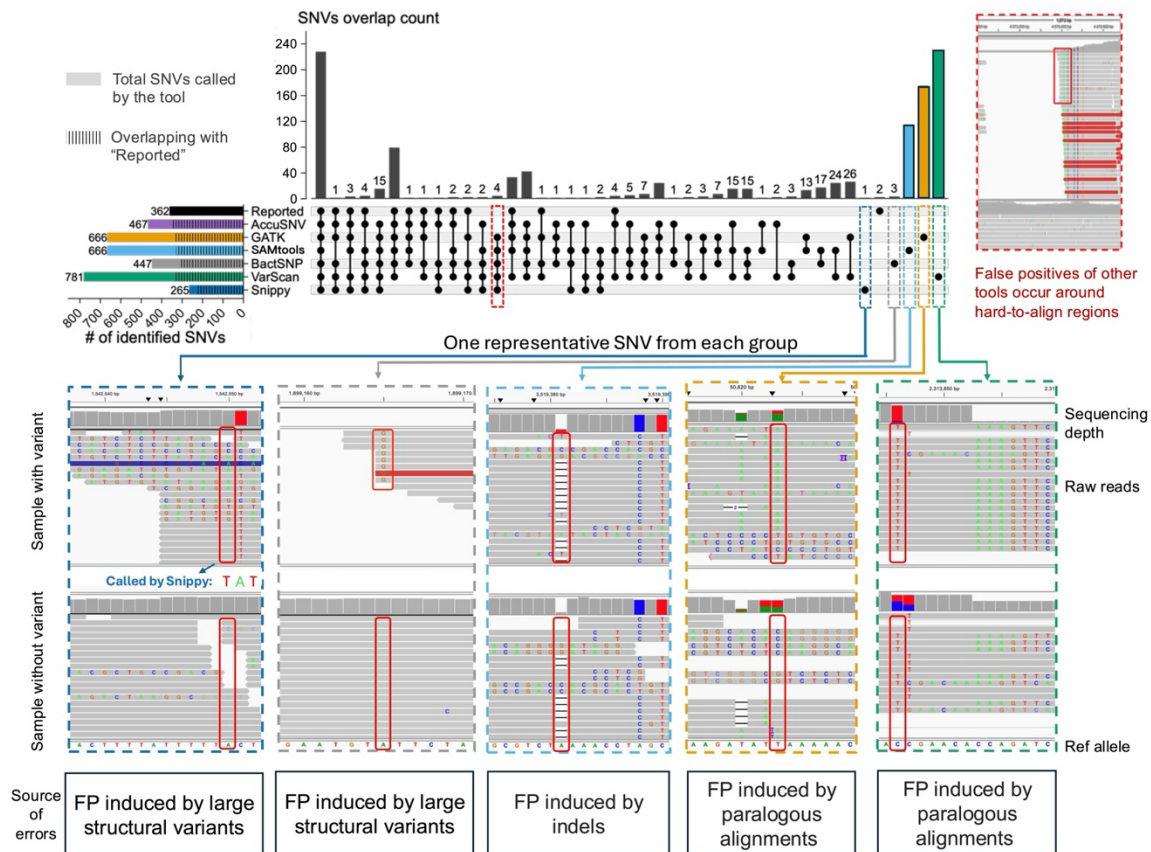
## 394 AccuSNV shows good robustness in simulated contaminated 395 samples

396 To assess the robustness of SNV calling tools under contamination, we simulated  
397 datasets with increasing levels of contamination, either from other strains of the  
398 same species or from closely related species, under both high and low sequencing  
399 depths. AccuSNV consistently achieved higher F1 scores than other tools in low-  
400 depth contaminated datasets and maintained perfect precision in all tested  
401 datasets. In high-depth settings (50× depth) with contamination from both other  
402 strains and closely related species, VarScan achieved the highest F1 scores across  
403 all datasets, with AccuSNV ranking second due to slightly lower recall. However, in  
404 this high-depth setting, when contamination originated from closely related  
405 species, VarScan exhibited reduced precision compared to AccuSNV. Full results  
406 are provided in Supplementary Section 2.1, Fig. S9-S12.

## 407 AccuSNV demonstrates high accuracy on real-world test data

408 Real-world data from independent studies, featuring diverse sequencing protocols,  
409 depths, species, and collection contexts, offer a more rigorous assessment for  
410 evaluating the robustness and accuracy in practical applications, as simulations  
411 rarely include all types of error and variability in the real world. In this experiment,  
412 we evaluated AccuSNV and other tools using four publicly available bacterial  
413 sequencing datasets (Snitkin et al. 2012; Giulieri et al. 2022; Kim et al. 2014; Buddle

414 et al. 2024), each derived from a distinct study, author group, and accompanied by  
 415 manually curated and reported SNVs that underwent careful quality control rather  
 416 than being taken directly from automated tool outputs. The four datasets differ in  
 417 read types (single-end vs. paired-end), bacterial species, and isolate numbers  
 418 (Supplementary Fig. S13). The dataset from Snitkin et al. (2012) comprises single-  
 419 end reads from a hospital outbreak of *Klebsiella pneumoniae*, while the others  
 420 involve paired-end sequencing of *Staphylococcus aureus* or *Clostridioides difficile*  
 421 collected under varying evolutionary or clinical contexts. These differences in  
 422 sequencing protocols, strain diversity, and sampling settings create a  
 423 heterogeneous and realistic benchmark for evaluating SNV-calling accuracy and  
 424 robustness.



426

426 **Figure 5. AccuSNV demonstrates high accuracy and precision on additional**  
 427 **real-world bacterial sequencing datasets.** We evaluated SNV concordance  
 428 between AccuSNV and five other tools across four published bacterial datasets with  
 429 curated SNVs (Supplementary Fig. S13). UpSet plots (center) display the SNVs  
 430 overlap count of tool-identified SNVs and reported SNVs. The red-outlined dash box  
 431 highlights a group of four SNVs identified by all tools except AccuSNV and the  
 432 original study (corresponding IGV (Robinson et al. 2011) screenshot is shown in the  
 433 top right panel). The IGV screenshot includes two sample tracks, one carrying the  
 434 reference allele and one carrying the alternative allele, with the variant position

435 *highlighted by a red box. Red reads indicate an inferred insert size larger than*  
436 *expected, which may suggest the presence of a deletion or a possible alignment*  
437 *artifact. The bottom panels display IGV screenshots of five unique SNVs identified*  
438 *by other methods but not supported by AccuSNV or the original study. The colored*  
439 *borders around each IGV screenshot correspond to the dashed boxes in the UpSet*  
440 *plot, indicating the group from which each SNV originated. Below each IGV*  
441 *screenshot is a description of the source of errors, highlighting typical error*  
442 *signatures such as misalignments near large structural variants, indels, and*  
443 *paralogous alignments. (as reported in (Koboldt 2020)). We note that these error*  
444 *modes are not generally tool specific, but that these tool-specific SNVs happen to*  
445 *have these error modes. Also see Supplementary Fig. S14-S17.*

446 All tools called distinct sets of SNVs across these data sets, with none matching the  
447 reported SNVs exactly (Fig. 5). Across all four datasets, AccuSNV demonstrates  
448 strong concordance with reported SNVs while minimizing tool-specific SNVs  
449 unsupported by other methods or the original studies (only 110 unreported SNVs,  
450 compared to 127-422 for other tools, except Snippy, which had 26 but identified  
451 much fewer reported SNVs).

452 Inspection of discordances among SNV calling methods illustrates that AccuSNV  
453 avoids false positives called by other tools, generally caused by alignment errors.  
454 For example, a notable group of SNVs is highlighted in the red dashed box (Fig. 5);  
455 these four SNVs from the same study were called by all other tools but not called by  
456 AccuSNV or the original study. To investigate the basis of this discrepancy, we  
457 visualized the corresponding BAM files of these four SNVs, one of which is shown in  
458 the panel outlined on the right. These four SNVs appear to be false positives located  
459 in hard-to-align regions, due to divergent regions between the sample and  
460 reference.

461 In addition, all tools except AccuSNV reported unique SNVs that were not  
462 supported by any other method or the original study. To further examine these  
463 unique SNVs, we manually reviewed five random unique SNVs from tested tools  
464 and visualized their read alignments (bottom panel of Fig. 5). In all cases, the  
465 alignments revealed problematic mapping features, such as soft clipping,  
466 inconsistent base support, or alignment gaps. These findings suggest that these  
467 unique SNVs called by other tools are false positives resulting from alignment  
468 errors. This observation agrees with previous studies, such as the one by Koboldt  
469 (2020) (Koboldt 2020), which identified similar artifacts in short read alignments  
470 leading to false-positive variant calls. While the IGV examples in Fig. 5 highlight  
471 representative alignment-related error modes, we further assessed whether these  
472 patterns generalize across datasets by quantifying site-level signatures associated  
473 with reported and unique SNVs for each variant caller. Across four real-world  
474 datasets, we observed that different callers exhibit distinct but dataset-dependent  
475 distributions of allele balance, sequencing depth, and mapping quality  
476 (Supplementary Fig. S14-S17). These results indicate that although certain error

477 modes recur, their quantitative manifestations vary substantially across datasets,  
478 complicating the use of universal hard filtering thresholds. In contrast, AccuSNV is  
479 able to filter these false positives by capturing informative across-sample features  
480 from alignment data, rather than relying on manually defined thresholds or manual  
481 filtering of individual positions.

## 482 Output and downstream analysis modules of AccuSNV

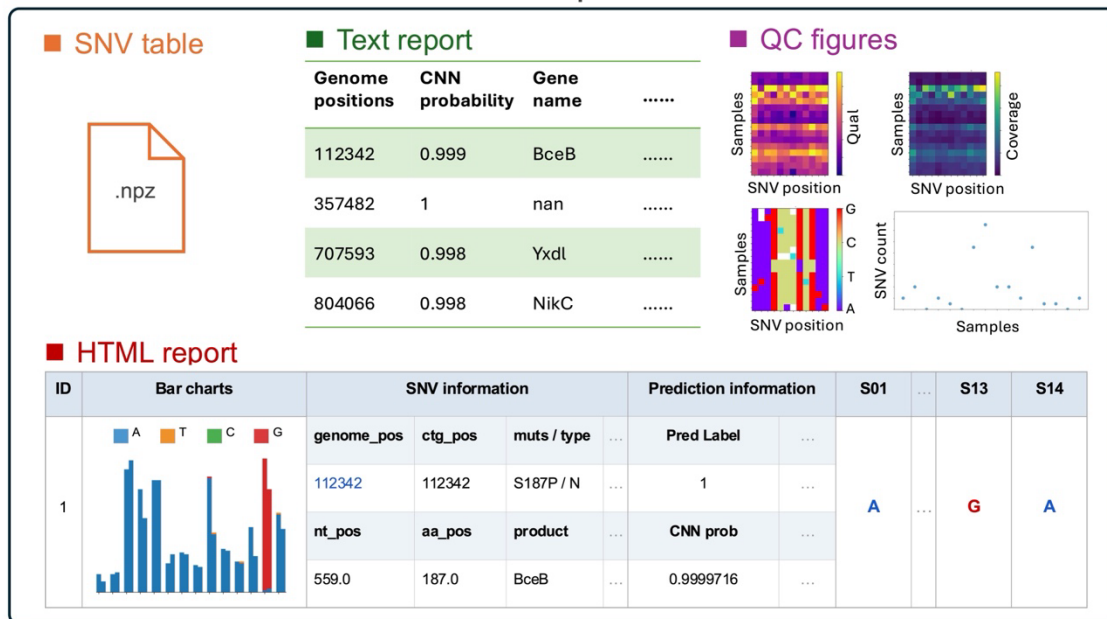
483 To support users with varying levels of computational expertise, AccuSNV offers  
484 comprehensive output and downstream analysis modules based on the identified  
485 SNVs. The core output includes a compressed SNV table in NumPy's .npz format (a  
486 compact binary file for storing arrays), a human-readable tab-separated summary  
487 of all the SNVs (TSV), including the allele call for each sample, a graphical HTML  
488 report, and a set of quality control (QC) figures (Fig. 6).

489 The HTML report provides an interactive platform for variant review. Each predicted  
490 SNV is visualized with a bar chart showing allele frequency distributions across  
491 isolates (as in Fig. 1), alongside detailed metadata such as strand-specific depth,  
492 mapping quality statistics, and various filter flags. A demo output HTML report can  
493 be found at <https://heruiliao.github.io/>. This design helps users assess variant  
494 confidence and identify potentially ambiguous cases that may require manual  
495 curation. In addition, AccuSNV generates multiple QC figures to assist in data  
496 quality assessment, including heatmaps of genome coverage and allele count  
497 distributions across samples. The human-readable tab-separated TSV file presents  
498 essential information for each SNV for rapid inspection and integration with external  
499 pipelines. Lastly, the compressed SNV Numpy table stores all variant-level features  
500 and prediction outputs in an efficient binary format, which serves as input for  
501 downstream modules.

502 To facilitate related applications, AccuSNV includes built-in modules for common  
503 downstream analyses. These modules enable manual filtering, phylogenetic tree  
504 construction, calculation of  $d_N/d_S$  ratios to assess selective pressures, and  
505 identification of homoplastic SNVs (Edwards et al. 2021). Additionally, users can  
506 export filtered variants for phylogenetic analysis with external tools.

507 Together, these outputs and utilities make AccuSNV a versatile and accessible tool  
508 for high-confidence bacterial SNV detection and interpretation.

## Output



509

510 *Figure 6. Output and downstream analysis modules of AccuSNV. The core outputs*  
 511 *include: (1). a compressed SNV table in NumPy's .npz format storing detailed*  
 512 *feature vectors and prediction scores, (2). a human-readable text summary file*  
 513 *(TSV) listing all identified SNVs with key attributes, (3). a set of quality control (QC)*  
 514 *figures summarizing read coverage, base calls, mapping quality scores, etc, (4). a*  
 515 *HTML report that integrates summary tables and bar charts of identified variants.*  
 516 *Homoplasic SNVs in the figure refers to variants where the same derived nucleotide*  
 517 *arises independently in two or more lineages since their divergence from a common*  
 518 *ancestor with a different ancestral base. These SNVs can be used to infer parallel,*  
 519 *convergent, or revertant evolutionary events (Edwards et al. 2021).*

520 **Discussion**

521 In this study, we present AccuSNV, a deep learning-based variant calling framework  
 522 designed for high-precision single nucleotide variant (SNV) detection from bacterial  
 523 whole-genome sequencing (WGS) data. By encoding multisample read alignment

524 data into structured feature vectors and leveraging a convolutional neural network  
525 (CNN), AccuSNV effectively captures across-sample patterns that are often ignored  
526 by conventional methods. Our approach addresses key challenges in bacterial  
527 variant calling, including low sequencing depth, high intraspecies diversity, and  
528 genome complexity. As a result, AccuSNV enables accurate bacterial SNV calling  
529 for users with varying levels of expertise, without the need for hard-coded  
530 thresholds or extensive manual filtering. While a few tools occasionally achieved  
531 comparable or better performance under specific conditions, AccuSNV was  
532 consistently the best or among the top-performing methods across all sequencing  
533 depths, reference and sequence divergence levels, and contamination scenarios  
534 (Figs. 3-5), demonstrating its broad applicability and scalability for bacterial  
535 genomics research. Interestingly, GATK performed as or nearly as well as AccuSNV  
536 under many conditions with default parameters on simulated data, likely because  
537 of its integration of across-sample comparisons (Fig. 3 and Fig. 4), but still had more  
538 identified false-positives when challenged with real world data (Fig. 5), likely due to  
539 structural variations between the reference and real samples. We note that all the  
540 tested pipelines can yield reliable results in many applied studies, particularly when  
541 users manually tune parameters, apply additional post hoc filtering, or visually  
542 inspect alignments, especially for high-depth datasets with closely related  
543 references. However, this reliance on dataset-specific decisions and expert  
544 judgment can limit reproducibility and scalability across large or heterogeneous  
545 cohorts, where systematic alignment-related error modes become more prominent  
546 (Yoshimura et al. 2019). AccuSNV minimizes manual parameter tuning by learning  
547 to identify false-positive SNVs directly from across-sample alignment patterns,  
548 enabling consistent performance across sequencing depths and reference  
549 divergence levels. Feature ablation analysis revealed that this robustness arises  
550 from integrating multiple complementary features rather than depending on any  
551 single signal, allowing the CNN to adapt to diverse sequencing conditions  
552 (Supplementary Fig. S4).

553 Despite these advances, AccuSNV has several limitations. First, the current  
554 implementation is designed and trained specifically for short-read sequencing data.  
555 Extending AccuSNV to long-read sequencing platforms such as Oxford Nanopore or  
556 PacBio would require retraining on platform-specific datasets and potentially  
557 incorporating features that capture their distinct error profiles. Second,  
558 misclassifications may still arise in extremely challenging or ambiguous cases  
559 encountered in real-world data, especially those involving false-positive SNVs  
560 arising from an error mode not represented in the training set. For example,  
561 although the training and test species span a broad range of genome sizes and GC  
562 content commonly observed in bacterial pathogens and commensals  
563 (Supplementary Table S2), AccuSNV has not yet been evaluated on bacteria with  
564 extreme genomic features (e.g., GC content <20% or >70%) or other haploid  
565 organisms such as yeast. To enable users to evaluate AccuSNV's performance on  
566 new use cases, AccuSNV provides an interactive HTML report and multiple quality

567 control visualizations that allow users to inspect candidate SNVs and flag potential  
568 false positives for downstream curation. Third, AccuSNV is specifically designed for  
569 SNV calling and does not currently support the identification of structural variants  
570 (SVs), such as insertions, deletions, or inversions. Fourth, the method is not directly  
571 applicable to metagenomic datasets, where a single sample may contain multiple  
572 closely related strains, resulting in more complex and ambiguous alignment  
573 patterns than those encountered in isolate-based WGS. Finally, while the across-  
574 sample alignment patterns that AccuSNV leverages to identify false positives may  
575 be consistent across organism types, the current implementation is limited to  
576 haploid genomes. Diploid genomes present a fundamentally different classification  
577 problem: distinguishing true heterozygous variants from sequencing or alignment  
578 errors, rather than simply identifying sites that deviate from a single reference  
579 allele.

580 We note that in all of our evaluation experiments, we assess each genomic position  
581 as either a true or false variant site, rather than evaluating individual per-sample  
582 variant calls. Thus, many individual false calls are reduced to only a single count in  
583 our evaluations. In practical applications, especially under low coverage or high  
584 reference divergence, many samples may have false-positives or false-negatives at  
585 a single position. As such, the position-level evaluation presented here provides a  
586 conservative benchmark of tool performance in these noisy and complex scenarios.

587 Looking forward, several directions can extend the utility of AccuSNV. One  
588 promising avenue is to expand the framework to support small indel detection by  
589 incorporating indel-aware features and labels during model training. Another  
590 direction is to explore whether across-sample alignment patterns in metagenomic  
591 data can be modeled to distinguish strain-specific SNVs, potentially enabling  
592 AccuSNV to operate in complex microbial communities. Extending the approach to  
593 diploid genomes is another promising direction that would require incorporating  
594 heterozygosity-aware features and training on datasets with appropriately labeled  
595 homozygous and heterozygous variants. However, these efforts may be constrained  
596 by the limited availability of real-world datasets with manually validated labels.

597 In conclusion, by reducing the need for manual thresholding and incorporating  
598 interpretable quality controls, AccuSNV makes high-confidence bacterial SNV  
599 calling accessible to users with varying levels of computational expertise. This  
600 accessibility makes it particularly well suited for studies of within-microbiome  
601 evolution, large-scale evolution experiments, and bacterial epidemiology, even  
602 when working with low-coverage or noisy sequencing data. By lowering technical  
603 barriers, AccuSNV enables broader adoption of high-precision SNV calling in  
604 diverse research and clinical settings.

## 605 Methods

### 606 Overview of AccuSNV

607 AccuSNV is designed for high-precision single nucleotide variant (SNV) calling from  
608 whole-genome sequencing data of bacterial isolates. It takes a reference genome  
609 and whole-genome sequencing short-read data from multiple bacterial samples  
610 (isolates) as input, and outputs identified SNVs along with associated information  
611 such as annotations, predicted probabilities, and visualization results, etc (Fig. 2  
612 and 6). AccuSNV leverages deep learning to distinguish true variants from  
613 sequencing or mapping artifacts, eliminating the need for manual filtering.  
614 Specifically, to address challenges such as low sequencing depth, genomic  
615 intraspecies diversity, variability in sample size, and sequencing quality across  
616 datasets, AccuSNV employs a CNN-based framework to learn informative patterns  
617 from multi-sample read alignment data. Here, we chose CNN for its ability to  
618 extract local features and maintain translation invariance (Lecun et al. 1998), which  
619 enables the robust detection of across-sample patterns from diverse and noisy  
620 bacterial isolate alignments. To implement this CNN-based approach, AccuSNV  
621 first identifies candidate SNV sites using SAMtools and extracts read-level features  
622 from bacterial isolate alignments using a Snakemake-based pipeline (Fig. 2A),  
623 including reads orientation, reads counting, mapping quality score, etc  
624 (Supplementary Fig. S1). These features are converted into a four-dimensional  
625 numerical feature vector, allowing the CNN to better capture both local and across-  
626 sample patterns. The CNN model (Fig. 2B) was trained using these four-  
627 dimensional feature vectors as input, and the final pretrained model is provided to  
628 perform binary SNV classification on new datasets.

### 629 Reference genomes used in this study

630 *Cutibacterium acnes* (C. *acnes* C1, GCF\_000302515.1), *Clostridium difficile* (C.  
631 *difficile* R20291, GCF\_000027105.1), *Escherichia coli* (E. *coli* str. K-12 substr.  
632 MG1655, GCF\_000005845.2), *Klebsiella pneumoniae* (K. *pneumoniae* subsp.  
633 *pneumoniae* NTUH-K2044, GCF\_000009885.1), *Staphylococcus aureus* (S. *aureus*  
634 subsp. *aureus* NCTC 8325, GCF\_000013425.1), *Streptococcus pneumoniae* (S.  
635 *pneumoniae* R6, GCF\_000007045.1) genomes were selected as reference genomes  
636 in this study.

### 637 Training and validation datasets

638 To train and evaluate the model, we collected a total of 7,638 “quality-filtered”  
639 SNVs (labeled as “True”) from 5,432 isolates from three datasets published in  
640 previous studies (Zhao et al. 2019; Conwill et al. 2022; Baker et al. 2025) conducted  
641 by our lab, and 6,306 “low-quality” SNVs filtered out during processing for these  
642 studies (labeled as “False”). These datasets comprise 222 lineages (finely resolved

643 clades separated by fewer than 100 mutations across the core genome (Conwill et  
 644 al. 2022; Baker et al. 2025)) and include carefully curated SNVs based on extensive  
 645 manual validation of filters in a study-specific manner. The criteria used in each  
 646 study to define “quality-filtered” SNVs are summarized in Supplementary Table S3.  
 647 To verify the collected positions in the training data, we randomly picked up to 10  
 648 true and 10 false positions per lineage (for a maximum of 20 per lineage), but some  
 649 lineages contained fewer than 20 available sites, resulting in 2,859 positions that  
 650 were manually inspected using generated bar charts (see example in Fig. 1). These  
 651 bar charts are available at <https://zenodo.org/records/17058222>. Manual  
 652 inspection confirmed that the assigned labels were accurate and consistent with  
 653 the expected patterns. These data were split into training and validation sets at an  
 654 4:1 ratio, stratified by lineages across the three datasets. This ensured that the  
 655 validation set contained isolates from different lineages and datasets, resulting in  
 656 10,887 SNVs for training and 3,057 SNVs for validation, and thereby improving the  
 657 generalizability of the trained model. Accession numbers and additional details  
 658 regarding the training data are provided in Supplementary Table S4. Additionally, to  
 659 assess tool performance on real-world data from independent studies, we  
 660 collected 362 reported SNVs from four different published datasets, where SNVs  
 661 had been carefully validated in the original studies through stringent filtering and  
 662 manual inspection rather than taken directly from automated tool outputs. Detailed  
 663 information on all seven datasets is provided in Table 1.

Datasets ID	Type	Species	# of lineages	# of isolates	# of True SNVs	# of False SNVs
Zhao_2019 (Zhao et al. 2019)	Training/V alidation	<i>B. fragilis</i>	11	556	227	492
Conwill_2022 (Conwill et al. 2022)		<i>C. acnes</i>	50	854	1,972	3,840
Baker_2025 (Baker et al. 2025)		<i>C. acnes</i>	85	2,007	3,444	554
		<i>S. epidermidis</i>	76	2,015	1,995	1,420
Kim_2014 (Kim et al. 2014)	Test	<i>S. aureus</i>	1	121	265	-
Buddle_2024 (Buddle et al. 2024)		<i>C. difficile</i>	1	96	55	-

Datasets ID	Type	Species	# of lineages	# of isolates	# of True SNVs	# of False SNVs
Snitkin_2012 (Snitkin et al. 2012)		<i>K. pneumoniae</i>	1	20	31	-
Giulieri_2022 (Giulieri et al. 2022)		<i>S. aureus</i>	1	16	11	-

664 *Table 1. Summary of the seven real bacterial whole-genome sequencing datasets*  
665 *used in this study. The first three datasets were used for model training and*  
666 *validation, while the remaining four served as independent test sets for additional*  
667 *evaluation. SNV calling was performed within lineages, defined as closely related*  
668 *clades identified based on core-genome similarity (Conwill et al. 2022; Baker et al.*  
669 *2025). “-” indicates no reported false SNVs in the original study.*

## 670 Identification of candidate SNVs

671 To identify candidate SNV sites from raw sequencing data, we implement a modular  
672 pipeline built with Snakemake (Mölder et al. 2025). The process begins with quality  
673 trimming of reads using cutadapt (v.1.18) (Martin 2011) and Sickle (Joshi and Fass  
674 2011) (v.1.33; -g -q 20 -l 50 -x -n), followed by reference-based alignment via BWA-  
675 MEM (Li and Durbin 2009) (v.0.7.18). Aligned reads are converted to sorted and  
676 indexed BAM files. SAMtools markdup (v.1.21.1; -r -s -d 100 -m s) is used to remove  
677 duplicate reads from each sample. Pileup and VCF files are then generated using  
678 SAMtools (Li et al. 2009) mpileup (v.1.21.1; -q30 -x -s -O -d3000), and BCFtools  
679 (Danecek et al. 2021) view (v.1.21.1; -Oz -v snps -q .75) . Critically, AccuSNV  
680 leverages Snakemake’s workflow management to automatically handle task  
681 dependencies and enable parallel execution of independent, sample-level  
682 preprocessing steps across multiple cores or cluster nodes when resources are  
683 available. This parallel execution strategy substantially reduces computational time  
684 compared to sequential preprocessing approaches, particularly for large datasets.  
685 As a result, while runtime scales approximately linearly with dataset size for tools  
686 that require predominantly sequential preprocessing (e.g., GATK), AccuSNV  
687 maintains efficient performance when scaling from tens to hundreds of isolates  
688 (Supplementary Table S1).

689 For each input sample, preliminary SNVs are extracted from VCF files and saved in  
690 compressed intermediate files. Then, the pipeline aggregates variant positions  
691 across all samples, and combines these positions with alignment-derived metrics,  
692 such as read counting and mapping quality score, into a candidate mutation table  
693 using custom Python scripts. This table contains informative alignment statistics for  
694 each candidate SNV and serves as the input for downstream analysis.

695 

## Feature extraction

696 To ensure the CNN can effectively capture informative patterns across bacterial  
 697 isolates, AccuSNV transforms raw alignment data into structured four-dimensional  
 698 feature vectors. Specifically, for each candidate SNV position, we aggregate  
 699 information from all reads supporting each allele in each sample, including base  
 700 counts on forward and reverse strands, mapping quality scores, and indel signals  
 701 (the number of reads supporting insertions and deletions, broadcast across the four  
 702 base channels per sample; Supplementary Fig. S1). Notably, these features were  
 703 selected because they are commonly used in the manual filtering step across  
 704 previous studies (Zhao et al. 2019; Conwill et al. 2022; Key et al. 2023) for  
 705 distinguishing “quality-filtered” SNVs from “low-quality” positions. In addition, we  
 706 incorporate two normalized coverage-based features,  $d_{i,j}^{\text{norm}}$  and  $r_{i,j}$ , to better  
 707 represent both across-position and across-sample variation. These two features  
 708 are computed separately for forward and reverse strands to retain strand-specific  
 709 information:

$$710 \quad d_{i,j}^{\text{norm}} = \frac{d_{i,j}}{\text{median}(D_i)}$$

711 where  $d_{i,j}$  is the raw read depth of sample  $i$  at site  $j$ , and  $\text{median}(D_i)$  is the median  
 712 depth across all positions in sample  $i$ .

$$713 \quad r_{i,j} = \frac{d_{i,j}}{\sum_{x=1}^n d_{x,j}}$$

714 Here,  $r_{i,j}$  refers to the proportion of read depth from sample  $i$  relative to the total  
 715 depth across all  $n$  samples at position  $j$ , serving as a relative coverage signal across  
 716 isolates.

717 During feature extraction, we further observed that certain low-quality positions  
 718 display extremely unbalanced coverage distributions, where the depth of the  
 719 putative minor allele is orders of magnitude lower than that of the major allele (see  
 720 Supplementary Fig. S18). Such unusual “gap cases” are underrepresented in the  
 721 training data and tend to be misclassified by the CNN. To ensure these extreme  
 722 cases are consistently represented, we introduced a normalization-based  
 723 adjustment in the feature encoding step, implemented through a Z-score  
 724 framework:

$$725 \quad Z = \frac{\bar{x}_1 - \bar{x}_2}{\sigma_1}$$

726 where  $\bar{x}_1$  and  $\bar{x}_2$  denote the normalized read depths ( $d_{i,j}^{\text{norm}}$ ) of the major-allele-  
 727 supporting and alternate-allele-supporting samples, respectively, and  $\sigma_1$  is the  
 728 standard deviation of normalized read depths among the major-allele-supporting  
 729 samples. The one-sided p-value is then calculated as:

$$730 \quad p = 1 - \Phi(|Z|)$$

731 where  $\Phi$  denotes the cumulative distribution function of the standard normal  
732 distribution. Positions with  $p < 0.01$  are flagged as gap cases, and the  
733 corresponding feature values are normalized to ensure consistent representation  
734 across isolates. This adjustment is fully integrated into the feature construction  
735 process, making the AccuSNV more robust to highly skewed depth profiles. We also  
736 conducted an ablation study on this normalization-based adjustment to evaluate  
737 its impact on performance (Supplementary Section 2.2). The results show that this  
738 design improves the robustness of AccuSNV on datasets containing positions with  
739 extreme coverage imbalance by reducing false positives while maintaining high  
740 recall (Supplementary Fig. S8).

741 These features are then encoded as a four-dimensional feature vector (Fig. 2),  
742 where the last dimension represents the nucleotide channels. This four-  
743 dimensional feature encoding has two key advantages over traditional feature  
744 representation like raw VCF statistics or flattened alignment matrices. First, it  
745 encodes comprehensive alignment features in a structured, image-like format that  
746 is well suited for the CNN model, enabling it to leverage translation invariance and  
747 local feature extraction. Second, it preserves across-sample information, enabling  
748 the model to capture shared or contrasting patterns among isolates at each site.  
749 These patterns are not accessible to conventional single-sample variant callers but  
750 are essential for distinguishing true SNVs from sequencing or alignment artifacts.

## 751 Deep learning framework

752 Given the extracted feature vectors, we employ a convolutional neural network to  
753 classify the candidate SNVs. There are two major challenges in applying CNN to this  
754 task. First, the number of bacterial isolates varies across datasets, leading to input  
755 tensors with different dimensions along the sample axis. Such variability poses a  
756 problem for standard CNN architectures, which require fixed input dimensions for  
757 training and inference. Second, compared to natural image tensors that often  
758 contain rich spatial information and high-dimensional features, our input tensors  
759 have a much lower feature dimensionality. Commonly used deep or parameter-  
760 heavy models are therefore prone to overfitting, especially given the limited number  
761 of labeled training examples.

762 To address these issues, we designed a CNN architecture to accommodate the  
763 varying alignment data. The model consists of convolutional, pooling, and fully  
764 connected layers (Fig. 2B). Specifically, we used three convolutional layers to  
765 hierarchically capture both localized signal structures and broader across-sample  
766 patterns. These three layers use 32, 64, and 128 filters with kernel sizes of  $3 \times 4$ ,  
767  $2 \times 1$ , and  $1 \times 1$ , respectively. Each convolutional layer is followed by a ReLU  
768 activation function. To accommodate inputs with variable sample sizes, we apply  
769 an adaptive average pooling operation (Hsin and Su 2021) along the sample axis,

770 compressing variable-length inputs into a fixed-size representation. Unlike standard  
 771 pooling layers with fixed kernel sizes, adaptive pooling dynamically divides the input  
 772 into regions such that the output always has the same predefined shape, regardless  
 773 of the input size. Let the  $\mathbf{X} \in \mathbb{R}^{x \times y \times z \times 4}$  be the input feature vector, where  $x$  is the  
 774 number of candidate SNV positions,  $y$  is the number of samples (bacterial isolates),  
 775  $z$  is the number of features, and 4 is the input channels. Then, the output tensor  $\mathbf{Z}$  of  
 776 the adaptive average pooling layer is:

$$777 \quad \mathbf{Z} = \text{AdaptiveAvgPool}(f_{\text{conv}}(\mathbf{X})), \mathbf{Z} \in \mathbb{R}^{x \times c \times 1 \times 1}$$

778 where  $c$  is the number of output channels from the last convolutional layer. This  
 779 operation enables the model to generalize across datasets with different sample  
 780 sizes while learning informative patterns across isolates. The output of the pooling  
 781 layer is fed into a fully connected layer with 64 units, followed by dropout ( $p = 0.5$ )  
 782 and a final sigmoid output node that produces the probability of the SNV being true.  
 783 By default, the classification cutoff is 0.5.

## 784 Model training

785 The model was trained using real-world bacterial whole-genome sequencing data  
 786 with curated labels obtained from previously published studies (Baker et al. 2025;  
 787 Zhao et al. 2019; Conwill et al. 2022), as summarized in Table 1. During training, the  
 788 binary cross-entropy loss function was used as the objective function.

$$789 \quad \mathcal{L} = -\frac{1}{N} \sum_{i=1}^N [y_i \log(\hat{y}_i) + (1 - y_i) \log(1 - \hat{y}_i)]$$

790 where  $y_i \in \{0,1\}$  is the true label of the  $i$ -th candidate SNV and  $\hat{y}_i \in (0,1)$  is the  
 791 predicted probability. We implemented the model using PyTorch, and trained it  
 792 using the Adam optimizer with a learning rate of 0.0001, a batch size of 32, and early  
 793 stopping based on validation loss. The model was trained for 150 epochs, and the  
 794 one with the lowest validation loss was saved for all classification tasks in our  
 795 evaluation experiments. The learning curve of the model training is shown in  
 796 Supplementary Fig. S19. To assess feature importance, we performed an ablation  
 797 study by masking individual feature groups (setting values to zero) and retraining the  
 798 model using the same hyperparameters and data splits (Supplementary Fig. S4).

## 799 Evaluation metrics

800 To evaluate the performance of different tools, we used five standard metrics:  
 801 accuracy, precision, recall, F1 score, and area under the curve (AUC). Let  $TP$ ,  $FP$ ,  
 802  $TN$  and  $FN$  denote the number of true positives, false positives, true negatives, and  
 803 false negatives, respectively. The evaluation metrics are defined as:

$$\begin{aligned}\text{Accuracy} &= \frac{TP + TN}{TP + TN + FP + FN} \\ \text{Precision} &= \frac{TP}{TP + FP} \\ \text{Recall} &= \frac{TP}{TP + FN} \\ \text{F1 score} &= \frac{2 \cdot \text{Precision} \cdot \text{Recall}}{\text{Precision} + \text{Recall}}\end{aligned}$$

804

805 AUC was calculated based on different models' predicted probabilities and reflects  
806 their ability to distinguish true SNVs from false ones across different decision  
807 thresholds.

## 808 Data sets

809 Real-world datasets used in this paper are all publicly available. Bar charts for the  
810 2,859 positions selected for manual label inspection are available at  
811 <https://zenodo.org/records/17058222>. A demo output HTML report of AccuSNV can  
812 be found at <https://heruiliao.github.io/>.

## 813 Code availability

814 The source code of AccuSNV is freely available at  
815 <https://github.com/liaohherui/AccuSNV> and as Supplemental Code. AccuSNV is  
816 also available via Bioconda at <https://anaconda.org/bioconda/accusnv>. The  
817 command lines for running other SNV calling tools are provided in the  
818 Supplemental Methods. The custom scripts necessary to reproduce the  
819 benchmarking experiments can be accessed at GitHub  
820 (<https://github.com/liaohherui/accusnv-eval>) and as Supplemental Code.

## 821 Competing interests

822 The authors declare no competing interests.

## 823 Acknowledgements

824 This work has been supported by MIT-Novo Nordisk Artificial Intelligence  
825 Postdoctoral Fellowship to HL, NIH grant 1DP2GM140922 and R35GM156282 to  
826 TDL. ILM, MF, and FMK were supported by the Max Planck Society. During the  
827 preparation of this work, the authors used ChatGPT (<https://chatgpt.com/>) in order  
828 to rephrase sentences. We thank members of the Lieberman Lab and Key Lab for  
829 helpful comments.

830 *Author contributions*

831 Methodology: HL, PT, AC, EQ, AHM, JSB, MF, ILM, FMK, TDL; Investigation: HL, AHM,  
832 TDL, LB; Funding acquisition: HL, TDL; Writing: HL, TDL.

833 **References**

834 Ahmed, Shams Forruque, Md. Sakib Bin Alam, Mahtabin Rodela Rozbu, et al. 2023.  
835 “Deep Learning Modelling Techniques: Current Progress, Applications, Advantages,  
836 and Challenges.” *Artificial Intelligence Review* 56 (11): 13521–617.  
837 <https://doi.org/10.1007/s10462-023-10466-8>.

838 Baker, Jacob S., Evan Qu, Christopher P. Mancuso, A. Delphine Tripp, Arolyn  
839 Conwill, and Tami D. Lieberman. 2025. “Intraspecies Dynamics Underlie the  
840 Apparent Stability of Two Important Skin Microbiome Species.” *Cell Host Microbe*  
841 33: 643–56. <https://doi.org/10.1016/j.chom.2025.04.010>.

842 Barrick, Jeffrey E, Geoffrey Colburn, Daniel E Deatherage, et al. 2014. “Identifying  
843 Structural Variation in Haploid Microbial Genomes from Short-Read Resequencing  
844 Data Using Breseq.” *BMC Genomics* 15: 1039. [https://doi.org/10.1186/1471-2164-](https://doi.org/10.1186/1471-2164-15-1039)  
845 [15-1039](https://doi.org/10.1186/1471-2164-15-1039).

846 Barrick, Jeffrey E., Dong Su Yu, Sung Ho Yoon, et al. 2009. “Genome Evolution and  
847 Adaptation in a Long-Term Experiment with Escherichia Coli.” *Nature* 461: 1243–47.  
848 <https://doi.org/10.1038/nature08480>.

849 Baumdicker, Franz, Gertjan Bisschop, Daniel Goldstein, et al. 2021. “Efficient  
850 Ancestry and Mutation Simulation with Msprime 1.0.” *Genetics* 220: iyab229.  
851 <https://doi.org/10.1093/genetics/iyab229>.

852 Buddle, Jessica E., Lucy M. Thompson, Anne S. Williams, et al. 2024. “Identification  
853 of Pathways to High-Level Vancomycin Resistance in Clostridioides Difficile That  
854 Incur High Fitness Costs in Key Pathogenicity Traits.” *PLOS Biology* 22 (8):  
855 e3002741. <https://doi.org/10.1371/journal.pbio.3002741>.

856 Bush, Stephen J. 2021. “Generalizable Characteristics of False-Positive Bacterial  
857 Variant Calls.” *Microbial Genomics* 7 (8): 000615.  
858 <https://doi.org/10.1099/mgen.0.000615>.

859 Bush, Stephen J, Dona Foster, David W Eyre, et al. 2020. “Genomic Diversity Affects  
860 the Accuracy of Bacterial Single-Nucleotide Polymorphism–Calling Pipelines.”  
861 *GigaScience* 9 (2): giaa007. <https://doi.org/10.1093/gigascience/giaa007>.

862 Conwill, Arolyn, Anne C. Kuan, Ravalika Damerla, et al. 2022. “Anatomy Promotes  
863 Neutral Coexistence of Strains in the Human Skin Microbiome.” *Cell Host Microbe*  
864 30 (2): 171–182.e7. <https://doi.org/10.1016/j.chom.2021.12.007>.

- 865 Danecek, Petr, James K Bonfield, Jennifer Liddle, et al. 2021. “Twelve Years of  
866 SAMtools and BCFtools.” *GigaScience* 10 (2): giab008.  
867 <https://doi.org/10.1093/gigascience/giab008>.
- 868 Edwards, David J., Sebastián Duchene, Bernard Pope, and Kathryn E. Holt. 2021.  
869 “SNPPar: Identifying Convergent Evolution and Other Homoplasies from Microbial  
870 Whole-Genome Alignments.” *Microbial Genomics* 7 (12): 000694.  
871 <https://doi.org/10.1099/mgen.0.000694>.
- 872 Fuchs, Sebastian A., Lisanna Hülse, Teresa Tamayo, Susanne Kolbe-Busch, Klaus  
873 Pfeffer, and Alexander T. Dilthey. 2024. “NanoCore: Core-Genome-Based Bacterial  
874 Genomic Surveillance and Outbreak Detection in Healthcare Facilities from  
875 Nanopore and Illumina Data.” *mSystems* 9 (11): e01080–24.  
876 <https://doi.org/10.1128/msystems.01080-24>.
- 877 Garrison, Erik, and Gabor Marth. 2012. *Haplotype-Based Variant Detection from*  
878 *Short-Read Sequencing*. arXiv. <https://doi.org/10.48550/arXiv.1207.3907>.
- 879 Giulieri, Stefano G, Romain Guérillot, Sebastian Duchene, et al. 2022. “Niche-  
880 Specific Genome Degradation and Convergent Evolution Shaping Staphylococcus  
881 Aureus Adaptation During Severe Infections.” *eLife* 11: e77195.  
882 <https://doi.org/10.7554/elife.77195>.
- 883 Goig, Galo A., Silvia Blanco, Alberto L. Garcia-Basteiro, and Iñaki Comas. 2020.  
884 “Contaminant DNA in Bacterial Sequencing Experiments Is a Major Source of False  
885 Genetic Variability.” *BMC Biology* 18 (1): 24. [https://doi.org/10.1186/s12915-020-](https://doi.org/10.1186/s12915-020-0748-z)  
886 [0748-z](https://doi.org/10.1186/s12915-020-0748-z).
- 887 Halachev, Mihail R, Jacqueline Z-M Chan, Chrystala I Constantinidou, et al. 2014.  
888 “Genomic Epidemiology of a Protracted Hospital Outbreak Caused by Multidrug-  
889 Resistant Acinetobacter Baumanniin Birmingham, England.” *Genome Medicine* 6  
890 (11): 70. <https://doi.org/s13073-014-0070-x>.
- 891 Hernández Medina, Ricardo, Svetlana Kutuzova, Knud Nor Nielsen, et al. 2022.  
892 “Machine Learning and Deep Learning Applications in Microbiome Research.” *ISME*  
893 *Communications* 2 (1): 98. <https://doi.org/10.1038/s43705-022-00182-9>.
- 894 Hsin, Hsi-Chin, and Chien-Kun Su. 2021. “Adaptive Pooling for Convolutional  
895 Neural Networks with Arbitrary Input Sizes.” *2021 IEEE 3rd Eurasia Conference on*  
896 *IOT, Communication and Engineering (ECICE)*, 196–98.  
897 <https://doi.org/10.1109/ecice52819.2021.9645730>.
- 898 Huang, Weichun, Leping Li, Jason R. Myers, and Gabor T. Marth. 2011. “ART: A Next-  
899 Generation Sequencing Read Simulator.” *Bioinformatics* 28 (4): 593–94.  
900 <https://doi.org/10.1093/bioinformatics/btr708>.

- 901 Joshi, NA, and JN Fass. 2011. *Sickle: A Sliding-Window, Adaptive, Quality-Based*  
902 *Trimming Tool for FastQ Files*. GitHub repository.
- 903 Key, Felix M., Veda D. Khadka, Carolina Romo-González, et al. 2023. “On-Person  
904 Adaptive Evolution of *Staphylococcus Aureus* During Treatment for Atopic  
905 Dermatitis.” *Cell Host Microbe* 31 (4): 593–603.e7.  
906 <https://doi.org/10.1016/j.chom.2023.03.009>.
- 907 Kim, Seungsoo, Tami D. Lieberman, and Roy Kishony. 2014. “Alternating Antibiotic  
908 Treatments Constrain Evolutionary Paths to Multidrug Resistance.” *Proceedings of*  
909 *the National Academy of Sciences* 111 (40): 14494–99.  
910 <https://doi.org/10.1073/pnas.1409800111>.
- 911 Koboldt, Daniel C. 2020. “Best Practices for Variant Calling in Clinical Sequencing.”  
912 *Genome Medicine* 12 (1): 91. <https://doi.org/10.1186/s13073-020-00791-w>.
- 913 Koboldt, Daniel C., Ken Chen, Todd Wylie, et al. 2009. “VarScan: Variant Detection  
914 in Massively Parallel Sequencing of Individual and Pooled Samples.” *Bioinformatics*  
915 25 (17): 2283–85. <https://doi.org/10.1093/bioinformatics/btp373>.
- 916 Lecun, Y., L. Bottou, Y. Bengio, and P. Haffner. 1998. “Gradient-Based Learning  
917 Applied to Document Recognition.” *Proceedings of the IEEE* 86 (11): 2278–324.  
918 <https://doi.org/10.1109/5.726791>.
- 919 Li, Heng, and Richard Durbin. 2009. “Fast and Accurate Short Read Alignment with  
920 Burrows–Wheeler Transform.” *Bioinformatics* 25 (14): 1754–60.  
921 <https://doi.org/10.1093/bioinformatics/btp324>.
- 922 Li, Heng, Bob Handsaker, Alec Wysoker, et al. 2009. “The Sequence Alignment/Map  
923 Format and SAMtools.” *Bioinformatics* 25 (16): 2078–79.  
924 <https://doi.org/10.1093/bioinformatics/btp352>.
- 925 Liao, Herui, Jiayu Shang, and Yanni Sun. 2023. “GDmicro: Classifying Host Disease  
926 Status with GCN and Deep Adaptation Network Based on the Human Gut  
927 Microbiome Data.” *Bioinformatics* 39 (12): btad747.  
928 <https://doi.org/10.1093/bioinformatics/btad747>.
- 929 Lopatkin, Allison J., Sarah C. Bening, Abigail L. Manson, et al. 2021. “Clinically  
930 Relevant Mutations in Core Metabolic Genes Confer Antibiotic Resistance.”  
931 *Science* 371 (6531): eaba0862. <https://doi.org/10.1126/science.aba0862>.
- 932 Martin, Marcel. 2011. “Cutadapt Removes Adapter Sequences from High-  
933 Throughput Sequencing Reads.” *EMBnet.journal* 17 (1): 10.  
934 <https://doi.org/10.14806/ej.17.1.200>.

- 935 McKenna, Aaron, Matthew Hanna, Eric Banks, et al. 2010. “The Genome Analysis  
936 Toolkit: A MapReduce Framework for Analyzing Next-Generation DNA Sequencing  
937 Data.” *Genome Research* 20 (9): 1297–303. <https://doi.org/10.1101/gr.107524.110>.
- 938 Min, Seonwoo, Byunghan Lee, and Sungroh Yoon. 2016. “Deep Learning in  
939 Bioinformatics.” *Briefings in Bioinformatics* 18: bbw068.  
940 <https://doi.org/10.1093/bib/bbw068>.
- 941 Mölder, Felix, Kim Philipp Jablonski, Brice Letcher, et al. 2025. “Sustainable Data  
942 Analysis with Snakemake.” *F1000Research* 10: 33.  
943 <https://doi.org/10.12688/f1000research.29032.3>.
- 944 Robinson, James T, Helga Thorvaldsdóttir, Wendy Winckler, et al. 2011. “Integrative  
945 Genomics Viewer.” *Nature Biotechnology* 29 (1): 24–26.  
946 <https://doi.org/10.1038/nbt.1754>.
- 947 Sayers, Eric W, Jeffrey Beck, Evan E Bolton, et al. 2024. “Database Resources of the  
948 National Center for Biotechnology Information in 2025.” *Nucleic Acids Research* 53  
949 (D1): D20–29. <https://doi.org/10.1093/nar/gkae979>.
- 950 Schrader, Sarah M., Hélène Botella, Robert Jansen, et al. 2021. “Multiform  
951 Antimicrobial Resistance from a Metabolic Mutation.” *Science Advances* 7 (35):  
952 eabh2037. <https://doi.org/10.1126/sciadv.abh2037>.
- 953 Seemann, Torsten. 2015. *Snippy: Fast Bacterial Variant Calling from NGS Reads*.  
954 GitHub repository.
- 955 Snitkin, Evan S., Adrian M. Zelazny, Pamela J. Thomas, et al. 2012. “Tracking a  
956 Hospital Outbreak of Carbapenem-Resistant *Klebsiella Pneumoniae* with Whole-  
957 Genome Sequencing.” *Science Translational Medicine* 4 (148): 148ra116.  
958 <https://doi.org/10.1126/scitranslmed.3004129>.
- 959 Yoshimura, Dai, Rei Kajitani, Yasuhiro Gotoh, et al. 2019. “Evaluation of SNP Calling  
960 Methods for Closely Related Bacterial Isolates and a Novel High-Accuracy Pipeline:  
961 BactSNP.” *Microbial Genomics* 5 (5): 000261.  
962 <https://doi.org/10.1099/mgen.0.000261>.
- 963 Yue, Jia-Xing, and Gianni Liti. 2019. “simuG: A General-Purpose Genome  
964 Simulator.” *Bioinformatics* 35 (21): 4442–44.  
965 <https://doi.org/10.1093/bioinformatics/btz424>.
- 966 Zhao, Shijie, Tami D. Lieberman, Mathilde Poyet, et al. 2019. “Adaptive Evolution  
967 Within Gut Microbiomes of Healthy People.” *Cell Host Microbe* 25 (5): 656–667.e8.  
968 <https://doi.org/10.1016/j.chom.2019.03.007>.

969 Zojer, Markus, Lisa N. Schuster, Frederik Schulz, Alexander Pfundner, Matthias  
970 Horn, and Thomas Rattei. 2017. "Variant Profiling of Evolving Prokaryotic  
971 Populations." *PeerJ* 5: e2997. <https://doi.org/10.7717/peerj.2997>.